Effect of the atomic orbital on the retrieval of the ionization time on the basis of a phase-of-phase attoclock: F^- ions as an example

Jian-Hong Chen [1], Haiyuan Yu,[2,3] and Hongchuan Du [2,3,*]

[1]*School of Electronic Engineering, Lanzhou City University, Lanzhou 730070, China*

[2]*School of Nuclear Science and Technology, Lanzhou University, Lanzhou 730000, China*

[3]*Key Laboratory of Special Function Materials and Structure Design, Ministry of Education, Lanzhou University, Lanzhou 730000, China*

(Received 12 March 2024; accepted 1 July 2024; published 17 July 2024)

Recently, the phase-of-phase (POP) attoclock scheme [reported in Nature Photon. **15**, 765 (2021)] has been used to investigate the tunneling dynamics of krypton atoms, encompassing the electron sub-barrier phase and amplitude. However, the impact of initial atomic orbitals on the POP attoclock spectroscopy remains largely unexplored. Here, we scrutinize the influence of initial atomic orbitals on the contrast and phase spectra of POP attoclock using F^- ions as a specific example. It is found that the initial atomic orbital significantly impacts the contrast spectrum of the POP attoclock and the detachment time of low-energy electrons retrieved by the POP attoclock via the preexponential factor. Particularly for orbitals p_+ and p_-, the difference of retrieved detachment time can exceed 300 attoseconds at some emission angles. But for high-energy electrons, the detachment time is almost independent of the initial atomic orbital and can be accurately retrieved by the POP attoclock. This work underscores the profound influence of initial atomic orbitals on the measurement accuracy of the POP attoclock, and holds great significance for advancing POP attoclock spectroscopy.

DOI: 10.1103/PhysRevA.110.013113

I. INTRODUCTION

Ultrafast detection of strong-field process stands as one of the primary objectives of attosecond science, and is the fundamental step of understanding many other strong-field phenomena, including high-order harmonic generation [1], above-threshold ionization [2], and nonsequential double ionization [3]. For this purpose, many experimental techniques have been well established, such as attosecond streaking camera [4–6], reconstruction of attosecond beating by interference of two-photon transition [7], attosecond transient absorption spectroscopy [8], and attoclock [9–15]. Meanwhile, many important properties of the ionization process have been also unveiled, such as tunneling time delay [9–13], tunneling exit velocity [16–20], and position [21].

In a standard attoclock experiment, atoms or molecules are ionized using a close-to-circularly polarized femtosecond laser pulse [9,10]. Once the electron is released at the peak value of the electric field, the ionization time can be directly mapped to the emission angle of photoelectrons in the polarization plane of laser field. For an 800 nm laser field, the time resolution of $\sim$7 as can be achieved for the emission angle of 1° [9,10]. Recently, the phase-of-phase (POP) attoclock scheme has emerged [22–25], which combines the attoclock technique with two-color POP spectroscopy [26–30]. This innovative approach claims to determine the ionization time of photoelectrons across the entire momentum distribution [29], and has successfully extracted sub-barrier phase and amplitude of the tunneling ionization process [22]. Most recently, Guo *et al.* confirmed that the mapping relation between the final momentum of the photoelectron and its ionization instant is not uniform in attoclock scheme, especially when the photoelectron is emitted in a direction close to the minimum yield [31]. Nevertheless, both the traditional attoclock and POP attoclock encounter challenges in disentangling the impact of the ionic Coulomb potential on the electron emission angle, which hinders the interpretation of attoclock experiments.

On the other hand, while noble gases are usually employed in attoclock experiments, the corresponding analyses often rely on the assumption of a *s*-electron initial state [13,14]. Recent works have brought to light the significant influence of initial atomic orbitals on the ionization process [25,32–41]. For example, there is pronounced circular dichroism in the strong-field ionization of atoms with initial orbitals having a magnetic quantum number of $m = 1$ or -1. [32–36]. Besides, electrons ionized from distinct atomic orbitals possess different initial momenta at the tunneling exit, resulting in observable differences in the final momentum distribution and attoclock offset angle [37–41]. However, it remains unanswered whether the atomic orbitals have an impact on the electron ionization time retrieved by the POP attoclock. In this work, we address this inquiry by focusing on F^- ions with *p*-electron initial states, in which the long-range Coulomb potential is inherently absent. We calculate the contrast and POP phase spectra of the POP attoclock for F^- ions with different initial orbitals, respectively. It is indicated that the contrast spectra significantly depend on atomic orbitals. By comparing the electron detachment time (i.e., the real part of

*Contact author: duhch@lzu.edu.cn

 ©2024 American Physical Society

saddle-point time) retrieved by the conventional attoclock with those retrieved from the POP attoclock, we demonstrate that the detachment time for high-energy electrons remains almost unaffected by the initial atomic orbital, and can be accurately retrieved by the POP attoclock. However, for low-energy electrons, the initial atomic orbital significantly influences the detachment time retrieved by the POP attoclock. The underlying physical mechanisms are also revealed.

The structure of this paper is outlined as follows. In Sec. II, we introduce the main theoretical methods, encompassing the strong-field approximation (SFA) model, and fundamental concepts and mathematical details of the POP attoclock. Subsequently, in Sec. III, we present the principal findings and discussions surrounding the contrast and phase spectra of POP attoclock. Finally, a summary is provided in Sec. IV. Throughout this work, atomic units are employed unless explicitly stated.

II. THEORETICAL METHODS

A. SFA model

In the SFA model, the direct transition probability amplitude from the atomic ground state to the continuum state is given by [2]

$$M(\boldsymbol{p}) = -i\int_{-\infty}^{\infty}\langle \boldsymbol{p}+\boldsymbol{A}(t)|\boldsymbol{r}\cdot\boldsymbol{E}(t)|\varphi_{nlm}\rangle \exp[iS(t)]dt, \quad (1)$$

where $\boldsymbol{E}(t)$ is the instantaneous laser electric field, and $\boldsymbol{A}(t) = -\int_{-\infty}^{t}\boldsymbol{E}(\tau)d\tau$ is the corresponding vector potential. $\varphi_{nlm}(\boldsymbol{r})$ is the ground-state wave function of atom. Here, n, l, and m are the principal, orbital, and magnetic quantum numbers, respectively. For F^- ions, the asymptotic form of the initial wave function $\varphi_{nlm}(\boldsymbol{r})$ can be given as follows [42–44]:

$$\varphi_{nlm}(\boldsymbol{r}) \underset{r\gg 1}{\approx} B\frac{\exp(-\kappa r)}{r}Y_{lm}(r), \quad (2)$$

where $\kappa = \sqrt{2I_p}$, $B = 0.7$ and $I_p = 3.401$ eV.

The classical action $S(t)$ of the electron can be written as

$$S(t) = \int_{-\infty}^{t}\left\{\frac{1}{2}[\boldsymbol{p}+\boldsymbol{A}(t')]^2 + I_p\right\}dt'. \quad (3)$$

Usually, $M(\boldsymbol{p})$ is obtained by numerically integrating over time. Alternatively, the transition amplitude can be calculated by the saddle-point method [2,42–49]. The direct electron amplitude is $M(\boldsymbol{p}) = i\sum_{t_s}\psi_0[\boldsymbol{p}+\boldsymbol{A}(t_s)]S'(t_s)\sqrt{\frac{2\pi}{-iS''(t_s)}}\exp[iS(t_s)]$. Here $\psi_0(\boldsymbol{p}) = \frac{C_{kl}}{\sqrt{2\kappa^3}}(\frac{p}{2\kappa})^l Y_{lm}(\theta_p,\varphi_p)\exp(-il\pi/2)\frac{\Gamma(l+2)}{\Gamma(l+3/2)}{}_2F_1(\frac{l}{2}+1,\frac{l}{2}+\frac{3}{2};l+\frac{3}{2};-\frac{p^2}{\kappa^2})$ [32,34]. ${}_2F_1$ is the Gaussian hypergeometric series. The saddle-point time t_s is the root of the saddle-point equation $[\boldsymbol{p}+\boldsymbol{A}(t_s)]^2 + 2I_p = 0$. Physically, the real part of t_s, i.e., $\mathrm{Re}(t_s)$, represents the electronic detachment time. $S(t) = -\int_{t_s}^{\infty}\{\frac{1}{2}[\boldsymbol{p}+\boldsymbol{A}(t')]^2 + I_p\}dt'$, and $S''(t_s) = -2\boldsymbol{E}(t_s)\cdot[\boldsymbol{p}+\boldsymbol{A}(t_s)]$ is its second derivative. Following the treatment in Ref. [34], one can obtain the analytical expression of the transition amplitude. In previous work, it has been found that the p state with $m = 0$ gives a negligible contribution to the ionization signal in the polarized plane of the circularly polarized field [48,50]. Thus, we focus on the initial p states with $m = \pm 1$ for F^- ions. The p state with $m = 0$ will not be discussed. For the initial states of F^- ions with $m = \pm 1$, $M(\boldsymbol{p})$ can be given by [47–49],

$$M(\boldsymbol{p}) \propto \sum_{t_s}\{[p_x + A_x(t_s)] \pm i[p_y + A_y(t_s)]\}\frac{\exp[i\Phi(t_s)]}{\sqrt{-i\Phi''(t_s)}}, \quad (4)$$

where "±" corresponds to the magnetic quantum numbers $m = \pm 1$. It is noted that $M(\boldsymbol{p}) \propto \exp[i\Phi(t_s)]/\sqrt{-i\Phi''(t_s)}$ is usually used for s- electron initial state [2,42].

In the attoclock scheme, the elliptically polarized laser electric field can be expressed as

$$\boldsymbol{E}(t) = \frac{E_0}{\sqrt{1+\varepsilon^2}}(\varepsilon\sin\omega t\,\hat{x} + \cos\omega t\,\hat{y}), \quad (5)$$

where ω is the angular frequency. E_0 is the amplitude of the laser field. ε is the ellipticity. $\hat{x}$ and $\hat{y}$ are the unit vectors of the laser polarization plane.

In the POP attoclock scheme, a weak circularly polarized second harmonic field is added to the electric field of Eq. (5). The synthesized electric field is

$$\boldsymbol{E}(t) = \frac{E_0}{\sqrt{1+\varepsilon^2}}[\varepsilon\sin\omega t + \xi\sin(2\omega t+\phi)]\hat{x} + \frac{E_0}{\sqrt{1+\varepsilon^2}}[\cos\omega t + \xi\cos(2\omega t+\phi)]\hat{y}, \quad (6)$$

where ϕ and ξ are the phase delay and amplitude ratio between the second harmonic field and fundamental laser field, respectively.

B. Brief introduction of POP attoclock

The POP attoclock combines the attoclock technique with two-color POP spectroscopy, in which a weak circularly polarized second harmonic field is added to the conventional attoclock. The mathematical details can be found in Refs. [22–30]. In this section, we briefly introduce the fundamental concepts and mathematical details of the POP attoclock to make the presentation self-contained. The main idea of the POP attoclock is to view the ionization probability $P(\boldsymbol{p},\phi)$ as a periodic function of the time delay ϕ. For s-electron state, the ionization probability for each momentum $\boldsymbol{p}$ can be assumed as [26–30]

$$P_0(\boldsymbol{p},\phi) \simeq P_0(\boldsymbol{p}) + \Delta P_0(\boldsymbol{p})\cos[\phi + \Phi_{\mathrm{POP}}(\boldsymbol{p})] + \cdots, \quad (7)$$

where $P_0(\boldsymbol{p})$ is the ionization probability without the perturbative second harmonic field. $\Delta P_0(\boldsymbol{p})$ is the contrast, and $\Phi_{\mathrm{POP}}(\boldsymbol{p})$ is the phase of phase ranging from $-\pi$ to π. In practice, $\Delta P_0(\boldsymbol{p})$ and $\Phi_{\mathrm{POP}}(\boldsymbol{p})$ can be extracted by performing fast Fourier transform on $P(\boldsymbol{p},\phi)$ with respect to ϕ. Mathematically, Eq. (7) can be viewed as the Fourier series expansion of the ionization probability [28]. Following Refs. [22–26], we only limit our discussions to the second term of Eq. (7), the higher-order terms including the nth harmonic phase of phase are neglected.

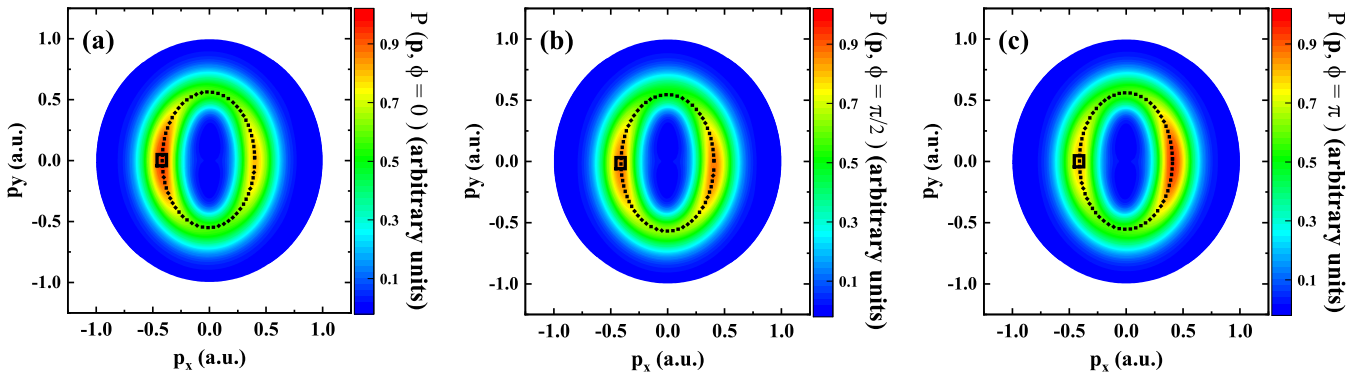

FIG. 1. Photoelectron momentum distributions of F^- ions with the initial orbital p_{+1} at different phase delays. (a) $\phi = 0$, (b) $\phi = \pi/2$, (c) $\phi = \pi$. The black squares denote the momentum $(p_x, p_y) = (-0.41, 0)$. The vector potential $\boldsymbol{A}(t)$ of the synthesized field is shown with the dashed line in each panel.

Actually, Eq. (7) can be easily derived by using the following approach: For the electric field in Eq. (6), its strength is

$$|\boldsymbol{E}(t)| = \frac{E_0}{\sqrt{1+\varepsilon^2}}\sqrt{[\varepsilon \sin\,\omega t\, + \xi \sin(2\omega t + \phi)]^2 + [\cos\,\omega t\, + \xi \cos(2\omega t + \phi)]^2} \tag{8}$$

and the strength of the fundamental field is

$$|\boldsymbol{E}_\omega(t)| = \frac{E_0}{\sqrt{1+\varepsilon^2}}\sqrt{\varepsilon^2 \sin^2\,\omega t\, + \cos^2\,\omega t}. \tag{9}$$

After dragging Eq. (9) into Eq. (8) and neglecting the second-order small quantity of ξ, Eq. (8) can be reduced to

$$|\boldsymbol{E}(t)| \approx |\boldsymbol{E}_\omega(t)| + \frac{\xi E_0}{\sqrt{1+\varepsilon^2}} \cos\,(2\omega t + \phi - \alpha_\omega), \tag{10}$$

where $\alpha_\omega = \arctan[\varepsilon \sin\,\omega t / \cos\,\omega t]$ is defined as the rotating angle of the attoclock pointer.

The photoelectron yield at the momentum $\boldsymbol{p}$ can be given by [22]

$$P(\boldsymbol{p}, \phi) \approx P_0(\boldsymbol{p}) + \frac{P_0(\boldsymbol{p})\xi E_0}{\sqrt{1+\varepsilon^2}} \cos(2\omega t + \phi - \alpha_\omega). \tag{11}$$

In the adiabatic limit, the tunnelling ionization rate is $\Gamma(t) \propto \exp[-2(2I_p)^{3/2}/3|E(t)|]$ [51]. In a standard attoclock experiment, atoms are ionized using a close-to-circularly polarized laser field, the ionization time can be directly linked with the photoelectron momentum. The photoelectron yield at the momentum $\boldsymbol{p}$ is closely related to the ionization rate at each ionization instant. By assuming $P_0(\boldsymbol{p}) \approx \exp[|E_\omega(t)|]$, one can easily derives Eq. (11) from Eq. (10). By comparing Eq. (11) with Eq. (7), we can see that the contrast is proportional to $P_0(\boldsymbol{p})$ and the phase of phase $\Phi_{\rm POP} = 2\omega t - \alpha_\omega$.

For the circularly polarized fundamental field ($\varepsilon = 1$), $\alpha_\omega = \omega t$ and $\Phi_{\rm POP} = \omega t$. The ionization time can be easily obtained by $t_i = \Phi_{\rm POP}/\omega$. However, for the elliptically polarized fundamental field, α_ω is not exactly equal to ωt. For example, α_ω can be expanded as $\alpha_\omega = \varepsilon\omega t + (\varepsilon - \varepsilon^3)\omega^3 t^3/3 + \cdots$ around $\omega t = 0$. When only retaining the first term, we can derive that $\Phi_{\rm POP} = 2\omega t - \varepsilon\omega t$ and the ionization time $t_i = \Phi_{\rm POP}/1.2\omega$ for $\varepsilon = 0.8$. Hence, strictly speaking, it is not very accurate to retrieve the ionization time by letting $\alpha_\omega \approx \omega t$ as in Ref. [22]. However, in this work, our goal is not to retrieve the exact ionization time, but to focus on the effects of initial atomic orbitals on the retrieval of ionization time in the POP attoclock. Therefore, we still adopt the approximation of $\alpha_\omega \approx \omega t$ in the implementation.

III. NUMERICAL RESULTS AND DISCUSSION

In order to study the effect of initial atomic orbital on the POP attoclock, we use a strong elliptically polarized fundamental field to drive the detachment of F^- ions, and a weak corotating circularly polarized second harmonic field to calibrate the detachment time. The intensity and wavelength of the fundamental field are 2×10^{13} W/cm^2 and 1500 nm, re-

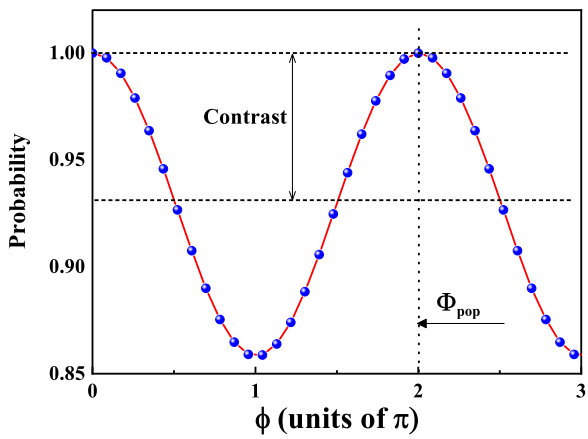

FIG. 2. Variation of photoelectron yield with the phase delay ϕ for a given photoelectron momentum marked with the black squares in Fig. 1. Two characteristic parameters of the yield oscillation, i.e., the contrast ΔP and POP phase $\Phi_{\rm POP}(\boldsymbol{p})$, are also given.

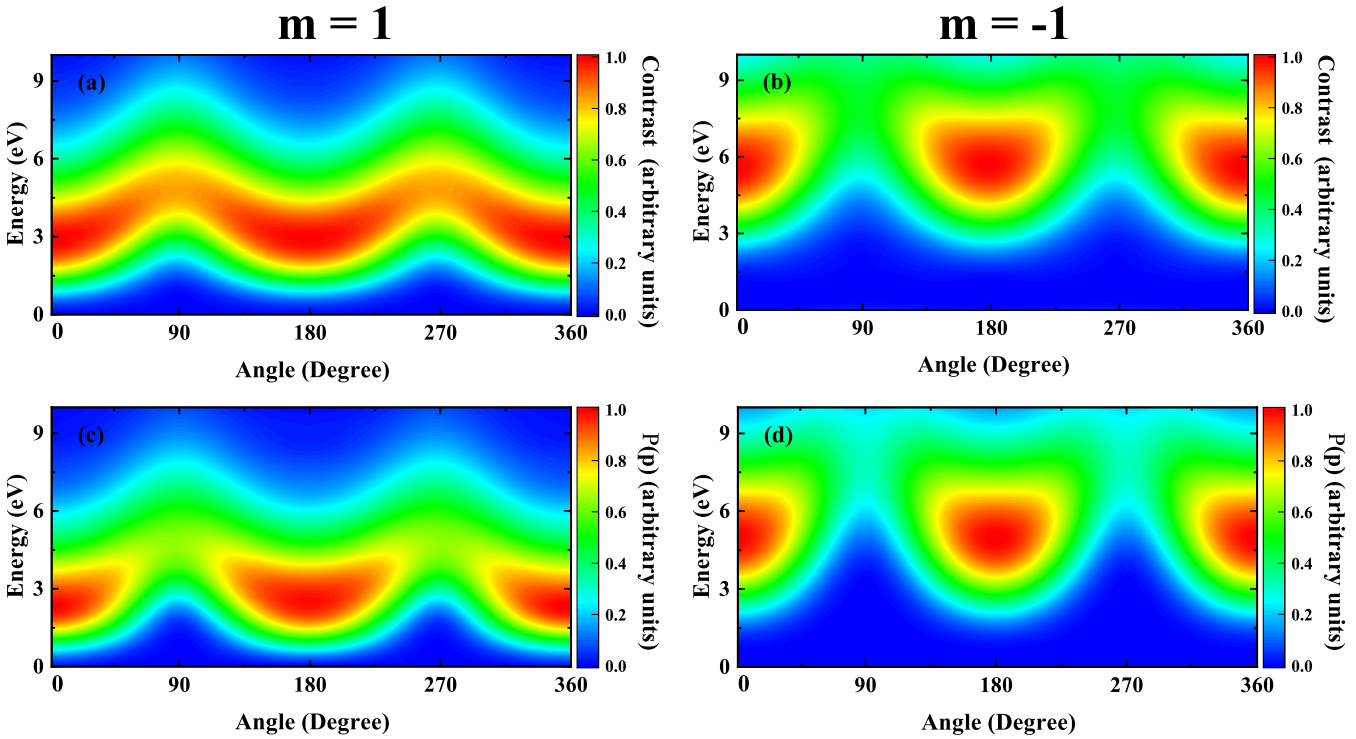

FIG. 3. (a) and (b) Contrast spectra of atomic orbitals p_{+1} and p_{-1}. (c) and (d) Corresponding PMDs calculated using the fundamental field. For clarify, the maximum values of spectra are normalized to 1.0.

spectively. The ellipticity is fixed at $\varepsilon = 0.8$. Correspondingly, the Keldysh parameter $\gamma = 0.635$, thus the electronic detachment is in the nonadiabatic tunneling regime. The amplitude ratio between the second harmonic field and fundamental laser field is set as $\xi = 0.01$, so that the detachment time is almost unaffected by the second harmonic field. To illustrate on the principle of POP attoclock, Fig. 1 shows the PMDs of F^- ions with the initial orbital p_{+1} at different phase delays. The vector potential $\boldsymbol{A}(t)$ of the synthesized field is shown with the dashed line in each panel. As shown, the overall momentum distribution follows the vector potential, and there are two obvious maxima near $\theta = 0^\circ$ and $\theta = 180^\circ$ in the PMDs. Moreover, the photoelectron yield strongly depends on the phase delay. When $\phi = 0$, the yield near $\theta = 180^\circ$ is larger than that near $\theta = 0^\circ$ as shown in Fig. 1(a). However, when $\phi = \pi$, the yield near $\theta = 180^\circ$ is less than that near $\theta = 0^\circ$, as seen in Fig. 1(c). To intuitively illustrate this tendency, Fig. 2 shows the variation of photoelectron yield with the phase delay. One can clearly see that the photoelectron yield oscillates with the phase delay in the form of a cosine function. The yield achieves the maximum when $\phi = 0$ or $\phi = 2\pi$, and has a minimum when $\phi = \pi$. Therefore, one can fit the yield with a standard cosine function, i.e., $P_0 + \Delta P \cos(\phi + \Phi_{\mathrm{POP}})$. Here, P_0 is background count, ΔP is the contrast, and Φ_{POP} is the phase of phase. The fitted curve is shown as the solid red line in Fig. 2. Two characteristic parameters ΔP and Φ_{POP} are also given. Finally, the contrast and POP spectra are extracted by the fast-Fourier transforming of the photoelectron yield $P(\boldsymbol{p}, \phi)$ with respect to ϕ for each momentum. The resolution of the phase delay is fixed as $\Delta\phi = \pi/12$. For each phase delay, we calculate the PMDs by the SFA model with numerical integration method. Note that we transform the coordinates (p_x, p_y) into the coordinates (angle, energy) by the relationship of angle $= \arctan(p_y/p_x)$ and energy $= (p_x^2 + p_y^2)/2$.

Next, we discuss the effect of initial atomic orbitals on the contrast of the POP attoclock. In Figs. 3(a) and 3(b), we present the contrast spectra of the POP attoclock for the initial orbitals p_{+1} and p_{-1}, respectively. It is found that the contrast spectra are strongly dependent on the atomic orbital, mainly manifested in the following two aspects. (i) The energy of the maximum photoelectron yield is different for different atomic orbitals. Specifically, the maximum yield appears around 3 eV and 6 eV for the orbitals p_{+1} and p_{-1}, respectively. (ii) The main structure of the contrast spectra dramatically depends on the atomic orbital. For the orbital p_{+1}, the contrast spectrum shows a M-shaped structure. However, for the orbital p_{-1}, the contrast spectrum consists of two V-shaped structures. Moreover, near $\theta = 90^\circ$ and $\theta = 270^\circ$, the contrast intensity

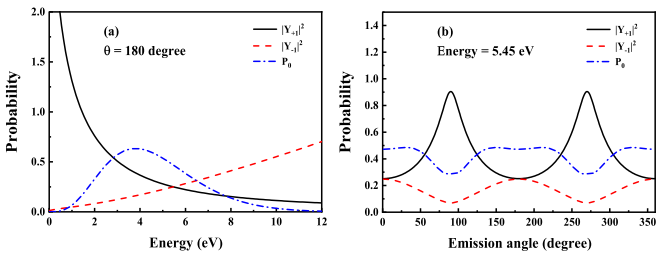

FIG. 4. $|Y_{+1}|^2$, $|Y_{-1}|^2$, and P_0 as functions of (a) energy for $\theta = 180^\circ$ and (b) angle for the energy of 5.45 eV.

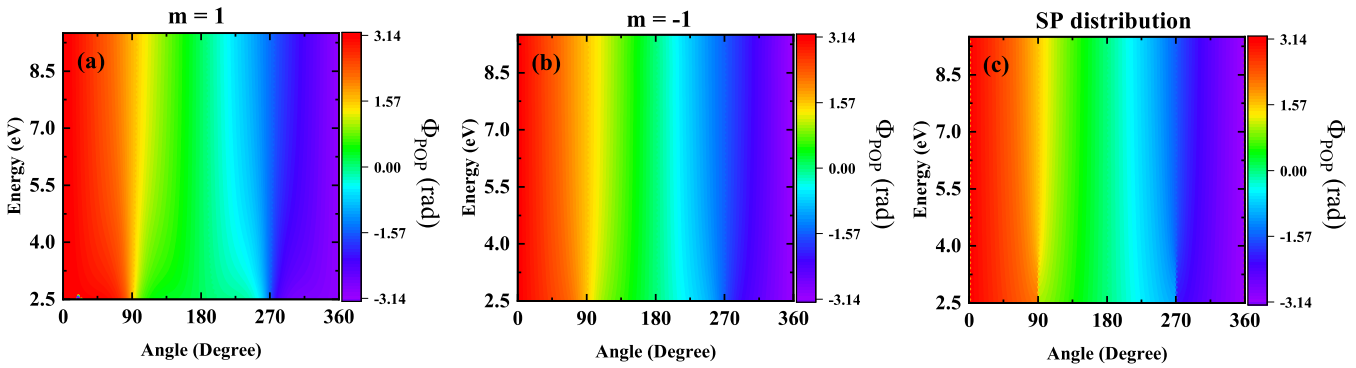

FIG. 5. Comparison of the extracted POP spectra with the saddle-point distribution. (a) POP spectrum of the orbital p_{+1}. (b) POP spectrum for the orbital p_{-1}. (c) Distribution of saddle-point time $\mathrm{Re}(\omega t_s)$.

of the orbital p_{+1} relative to its maximum is much larger than that of the orbital p_{-1}. For comparison, we also calculate the PMDs of the fundamental field using the SFA model, and the results are shown in Figs. 3(c) and 3(d). On the whole, the PMDs of the fundamental field are consistent with the contrast spectra, which coincides with the expectation of Eq. (11). This indicates that the initial atomic orbitals indeed affect the contrast spectrum of POP attoclock. Here, we briefly explain the reason why the contrast spectra depend on the atomic orbital. Based on Eq. (4), the preexponential factors for orbitals $p_{\pm1}$ are proportional to $Y_{\pm1} = [p_x + A_x(t_s)] \pm i[p_y + A_y(t_s)]$, while the ionization probability for s-electron state is proportional to $P_0 = |\exp[iS(t_s)]/\sqrt{-iS''(t_s)}|^2$. Figure 4 shows the variations of $|Y_{+1}|^2$, $|Y_{-1}|^2$, and P_0 with energy and angle, respectively. In Fig. 4(a), we fix the emission angle $\theta = 180°$. As shown, $|Y_{+1}|^2$ monotonically decreases with the electron energy, but $|Y_{-1}|^2$ monotonically increases with the electron energy, which leads to the energy difference of the maximum photoelectron yield for p_{+1} and p_{-1} (i.e., $|Y_{+1}|^2 P_0$ and $|Y_{-1}|^2 P_0$). When the energy is fixed, as shown in Fig. 4(b), $|Y_{-1}|^2$ and P_0 are much weaker dependent on θ than that for $|Y_{+1}|^2$, thus the main structure of the PMD for orbital p_{-1} (i.e., $|Y_{-1}|^2 P_0$) is similar to that of P_0, and strikingly different from the PMD for the orbital p_{+1} (i.e., $|Y_{+1}|^2 P_0$).

Figure 5 shows the orbital-resolved POP spectra. For comparison, the distribution of the saddle-point time $\mathrm{Re}(\omega t_s)$ is also given. Here, the saddle-point time $t_s(\boldsymbol{p})$ is obtained by numerically solving the saddle-point equation in the fundamental field. Note that there are two different saddle-point times $t_s(\boldsymbol{p})$ for each momentum $\boldsymbol{p}$. We choose the saddle-point time with less imaginary part, since it contributes to greater detachment probability. As a whole, the extracted POP spectra agree roughly with the distribution of the saddle-point time for two different orbitals. To highlight the influence of atomic orbitals on detachment time, we further plot the variation of detachment time with the emission angle in Fig. 6. For comparison, the detachment time for s-electron initial state is also presented. As shown in Fig. 6(a), the detachment time strongly depends on the atomic orbital except for four special angles, i.e., 0°, 90°, 180°, and 270°, when the electron energy is fixed at 3.2 eV. Particularly for orbitals p_{+1} and p_{-1}, the difference can exceed 300 attoseconds at some emission angles, e.g., 66°, 110°, 240°, and 290°. But, when the electron energy is 5.7 eV, the dependence of detachment time on the orbital significantly weakens, as seen in Fig. 6(b). Therefore, the effect of the initial atomic orbital needs to be carefully addressed for low-energy electrons in the POP attoclock. However, for high-energy electrons, the detachment time is almost independent of the initial atomic orbital and can be accurately retrieved by the POP attoclock.

Next, we discuss the physics for these differences observed in Fig. 6. Based on the previous work by Barth and Smirnova [34], the preexponential factor for orbitals $p_{\pm1}$ are proportional to $Y_{\pm1} = [p_x + A_x(t_s)] \pm i[p_y + A_y(t_s)]$, while the ionization probability for s-electron state is proportional to $P_0 = |\exp[iS(t_s)]/\sqrt{-iS''(t_s)}|^2$. Since the amplitude ratio between the second harmonic field and fundamental laser field is set as $\xi = 0.01$, the complex detachment time t_s is weakly dependent on the phase delay ϕ. However, the situation is different for $|Y_{+1}|^2$, $|Y_{-1}|^2$, and P_0. In Fig. 7, we show the variations of $|Y_{+1}|^2$, $|Y_{-1}|^2$, and P_0 with ϕ when the emission angle is fixed at $\theta = 66°$. As shown in Fig. 7(a), when the energy is fixed at 3.2eV, $|Y_{-1}|^2$ and P_0 are much weaker dependent on ϕ than $|Y_{+1}|^2$, thus $|Y_{+1}|^2$ effectively modulates the dependence of P_0 on ϕ. When the energy is fixed at 5.7 eV, P_0 is much stronger dependent on ϕ than $|Y_{+1}|^2$ and $|Y_{-1}|^2$, thus P_0 dominates the dependence of photoelectron yield on ϕ. Therefore, we believe that the dependence of $|Y_{+1}|^2$, $|Y_{-1}|^2$,

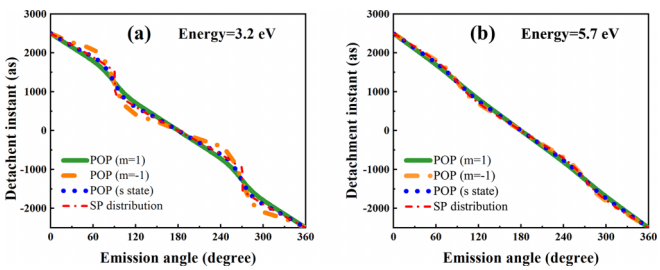

FIG. 6. Variation of detachment time with the emission angle when (a) energy = 3.2 eV and (b) energy = 5.7 eV.

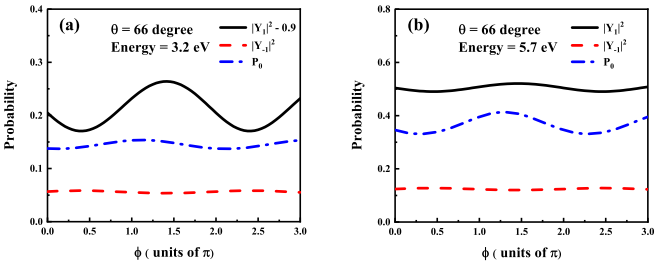

FIG. 7. Variations of $|Y_{+1}|^2$, $|Y_{-1}|^2$, and P_0 with ϕ when the emission angle is fixed at $\theta = 66^\circ$.

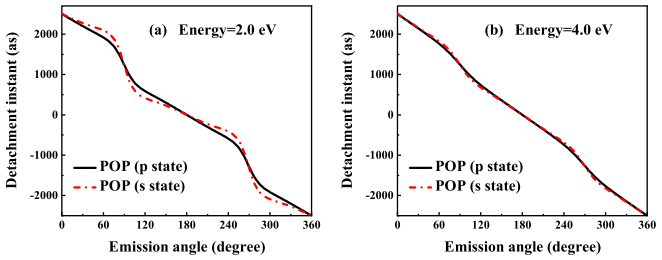

FIG. 8. Comparison of the detachment times for p state and s state when (a) energy = 2.0 eV and (b) energy = 4.0 eV.

and P_0 on ϕ are crucial for understanding these differences observed in Fig. 6.

To confirm the above idea, we rewrite the change of $|Y_{\pm1}|^2$ with the time delay ϕ as

$$|Y_{\pm1}|^2(\boldsymbol{p},\phi) \simeq \Upsilon_{\pm1}(\boldsymbol{p}) + \Delta\Upsilon_{\pm1}(\boldsymbol{p})\cos(\phi + \Phi_{\pm1}) + \cdots, \tag{12}$$

where $\Phi_{\pm1}$ represents the phase of phase when only considering the preexponential factor of p-electron state. By combining Eq. (7) and Eq. (12) and neglecting the higher-order terms, we obtain the orbital-resolved photoelectron yield as follows,

$$\begin{aligned} P_{\pm1}(\boldsymbol{p},\phi) \simeq\ & P_0(\boldsymbol{p})\Upsilon_{\pm1}(\boldsymbol{p}) \\ & + \Delta P_0(\boldsymbol{p})\Upsilon_{\pm1}(\boldsymbol{p})\cos[\phi + \Phi_{\mathrm{POP}}(\boldsymbol{p})] \\ & + \Delta\Upsilon_{\pm1}(\boldsymbol{p})P_0(\boldsymbol{p})\cos[\phi + \Phi_{\pm1}(\boldsymbol{p})], \end{aligned} \tag{13}$$

where $\Phi_{\mathrm{POP}}(\boldsymbol{p})$ is the phase of phase for the s-electron state in previous work [22].

Usually, $\Delta P_0(\boldsymbol{p})\Upsilon_{\pm1}(\boldsymbol{p}) > \Delta\Upsilon_{\pm1}(\boldsymbol{p})P_0(\boldsymbol{p})$, so $P_0(\boldsymbol{p},\phi)$ dominates the dependence of photoelectron yield on ϕ, and $|Y_{\pm1}|^2(\boldsymbol{p},\phi)$ modulates this dependence. If $\Delta P_0(\boldsymbol{p})\Upsilon_{\pm1}(\boldsymbol{p}) \gg \Delta\Upsilon_{\pm1}(\boldsymbol{p})P_0(\boldsymbol{p})$ is fulfilled, the third term of Eq. (13) can be reasonably removed, which means that the detachment time is independent on the initial atomic orbital. Through fitting $P_0(\boldsymbol{p},\phi)$ and $|Y_{\pm1}|^2(\boldsymbol{p},\phi)$ with a standard cosine function of ϕ, we can easily obtain the parameters in Eq. (13). For example, when the electron energy and emission angle θ are, respectively, equal to 3.2 eV and 66°, we obtain $P_0 = 0.145$, $\Delta P_0 = 0.008$, $\Phi_{\mathrm{POP}} = 159^\circ$; $\Upsilon_{+1} = 1.12$, $\Delta\Upsilon_{+1} = 0.046$, $\Phi_{+1} = 107^\circ$; $\Upsilon_{-1} = 0.056$, $\Delta\Upsilon_{-1} = 0.0023$, $\Phi_{-1} = 287^\circ$. Here, $\Delta P_0(\boldsymbol{p})\Upsilon_{\pm1}(\boldsymbol{p}) > \Delta\Upsilon_{\pm1}(\boldsymbol{p})P_0(\boldsymbol{p})$ is fulfilled, so $|Y_{\pm1}|^2(\boldsymbol{p},\phi)$ effectively modulates the dependence of $P_{\pm}(\boldsymbol{p},\phi)$ on ϕ, affecting the measurement accuracy of the POP attoclock as shown in Fig. 6(a). When the electron energy and emission angle θ are, respectively, equal to 5.7 eV and 66°, the difference between $\Delta P_0(\boldsymbol{p})\Upsilon_{\pm1}(\boldsymbol{p})$ and $\Delta\Upsilon_{\pm1}(\boldsymbol{p})P_0(\boldsymbol{p})$ obviously increases, which significantly weakens the modulation effect of $|Y_{\pm1}|^2(\boldsymbol{p},\phi)$. Thus, as shown in Fig. 6(b), the detachment time is almost independent of the initial atomic orbital.

In experiments, there is always a mixture of p_0, p_{-1}, and p_{+1} orbials. Hence, we further give the orbital-averaging detachment time for p-electron initial state in Fig. 8. The detachment probability $P(\boldsymbol{p})$ for p-electron initial state is obtained by $P(\boldsymbol{p}) = [P_{m=0}(\boldsymbol{p}) + P_{m=1}(\boldsymbol{p}) + P_{m=-1}(\boldsymbol{p})]/3$. For comparison, the detachment time for s-electron initial state is also presented. As shown in Fig. 8(a), the detachment time still strongly depends on the initial state except for four special angles, when the electron energy is 2.0 eV. However, when the electron energy is increased to 4.0 eV, the dependence of detachment time on the initial state becomes not obvious, as seen in Fig. 8(b). This indicates that even considering the orbital-averaging effect, the influence of the initial orbital on the retrieval ionization time could be observed for the low-energy detachment electrons in the experiment.

For the neutral atoms with p-electron initial state, their unique difference from F^- ions is the presence of the Coulomb potential. So, we can infer that for the neutral atoms with p-electron initial state, the ionization time retrieved by the POP attoclock should also depend on the atomic orbital in low-energy region. Meanwhile, there are also the above special angles, although they may be shifted from 0°, 90°, 180°, and 270° due to the Coulomb field. Finally, it should be emphasized that the above special angles are only limited to the negative ions and the neutral atoms with p-electron initial states. For other atoms with more complex structures, these angles may also vary.

IV. CONCLUSIONS

In summary, we theoretically investigate the effect of atomic orbital on the contrast and POP spectra of POP attoclock, taking F^- ions as an example. It is found that the contrast spectra show similar structures with the PMDs of the fundamental field, and dramatically depend on the initial orbital. Additionally, we confirm the substantial impact of the atomic orbital on the mapping relation between electron momentum and detachment time. But at some specific angles or for high-energy electrons, the mapping relation is proved to be nearly independent of atomic orbitals. Through the saddle-point method, we demonstrate how the preexponential factor take effect on the dependence of the POP spectrum on the initial orbital. Given the importance of the mapping relation between electron momentum and detachment time in characterizing tunneling dynamics, this work is of great significance for investigating the electron ionization dynamics of negative ions with valence p orbitals and even noble-gas atoms.

ACKNOWLEDGMENTS

We sincerely thank Prof. Yunquan Liu and Prof. Liang-You Peng in Peking University of China, and Professor

Meng Han in Kansas State University of the U.S.A for providing very valuable help and suggestions for this work. This work is supported by the National Natural Science Foundation of China (Grants No.12064023, No. 12274188, No. 12204209), the Natural Science Foundation of Gansu Province (Grant No. 20JR5RA209), and the Fundamental Research Funds for the Central Universities (Grant No. lzujbky-2023-ey08).

[1] F. Krausz and M. Ivanov, Attosecond physics, Rev. Mod. Phys. **81**, 163 (2009).

[2] D. B. Milošević, G. G. Paulus, D. Bauer, and W. Becker, Above-threshold ionization by few-cycle pulses, J. Phys. B: At. Mol. Opt. Phys. **39**, R203 (2006).

[3] W. Becker, X. J. Liu, P. J. Ho, and J. H. Eberly, Theories of photoelectron correlation in laser-driven multiple atomic ionization, Rev. Mod. Phys. **84**, 1011 (2012).

[4] J. Itatani, F. Quéré, G. L. Yudin, M. Y. Ivanov, F. Krausz, and P. B. Corkum, Attosecond streak camera, Phys. Rev. Lett. **88**, 173903 (2002).

[5] E. Goulielmakis, M. Uiberacker, R. Kienberger, A. Baltuska, V. Yakovlev, A. Scrinzi, T. Westerwalbesloh, U. Kleineberg, U. Heinzmann, M. Drescher, and F. Krausz, Direct measurement of light waves, Science **305**, 1267 (2004).

[6] G. Sansone, E. Benedetti, F. Calegari, C. Vozzi, L. Avaldi, R. Flammini, L. Poletto, P. Villoresi, C. Altucci, R. Velotta, S. Stagira, S. de Silvestri, and M. Nisoli, Isolated singlecycle attosecond pulses, Science **314**, 443 (2006).

[7] P. M. Paul, E. S. Toma, P. Breger, G. Mullot, F. Augé, P. Balcou, H. G. Muller, and P. Agostini, Observation of a train of attosecond pulses from high harmonic generation, Science **292**, 1689 (2001).

[8] E. Goulielmakis, Z.-H. Loh, A. Wirth, R. Santra, N. Rohringer, V. S. Yakovlev, S. Zherebtsov, T. Pfeifer, A. M. Azzeer, M. F. Kling, S. R. Leone, and F. Krausz, Real-time observation of valence electron motion, Nature (London) **466**, 739 (2010).

[9] P. Eckle, M. Smolarski, P. Schlup, J. Biegert, A. Staudte, M. Schöffler, H. G. Muller, R. Dörner, and U. Keller, Attosecond angular streaking, Nature Phys. **4**, 565 (2008).

[10] P. Eckle, A. N. Pfeiffer, C. Cirelli, A. Staudte, R. Dörner, H. G. Muller, M. Büttiker, and U. Keller, Attosecond ionization and tunneling delay time measurements in helium, Science **322**, 1525 (2008).

[11] L. Torlina, F. Morales, J. Kaushal, I. Ivanov, A. Kheifets, A. Zielinski, A. Scrinzi, H. G. Muller, S. Sukiasyan, M. Ivanov, and O. Smirnova, Interpreting attoclock measurements of tunnelling time, Nature Phys. **11**, 503 (2015).

[12] U. S. Sainadh, H. Xu, X. Wang, A. Atia-Tul-Noor, W. C. Wallace, N. Douguet, A. Bray, I. Ivanov, K. Bartschat, A. Kheifets, R. T. Sang, and I. V. Litvinyuk, Attosecond angular streaking and tunnelling time in atomic hydrogen, Nature (London) **568**, 75 (2019).

[13] N. Camus, E. Yakaboylu, L. Fechner, M. Klaiber, M. Laux, Y. Mi, K. Z. Hatsagortsyan, T. Pfeifer, C. H. Keitel, and R. Moshammer, Experimental evidence for quantum tunneling time, Phys. Rev. Lett. **119**, 023201 (2017).

[14] M. Han, P. Ge, Y. Fang, X. Yu, Z. Guo, X. Ma, Y. Deng, Q. Gong, and Y. Liu, Unifying tunneling pictures of strong-field ionization with an improved attoclock, Phys. Rev. Lett. **123**, 073201 (2019).

[15] N. Eicke, S. Brennecke, and M. Lein, Attosecond-scale streaking methods for strong-field ionization by tailored fields, Phys. Rev. Lett. **124**, 043202 (2020).

[16] O. Pedatzur, G. Orenstein, V. Serbinenko, H. Soifer, B. D. Bruner, A. J. Uzan, D. S. Brambila, A. G. Harvey, L. Torlina, F. Morales, O. Smirnova, and N. Dudovich, Attosecond tunnelling interferometry, Nature Phys. **11**, 815 (2015).

[17] M. Li, M. M. Liu, J. W. Geng, M. Han, X. Sun, Y. Shao, Y. Deng, C. Wu, L. Y. Peng, Q. Gong, and Y. Liu, Experimental verification of the nonadiabatic effect in strong-field ionization with elliptical polarization, Phys. Rev. A **95**, 053425 (2017).

[18] S. Eckart, K. Fehre, N. Eicke, A. Hartung, J. Rist, D. Trabert, N. Strenger, A. Pier, L. P. H. Schmidt, T. Jahnke, M. S. Schöffler, M. Lein, M. Kunitski, and R. Dörner, Direct experimental access to the nonadiabatic initial momentum offset upon tunnel ionization, Phys. Rev. Lett. **121**, 163202 (2018).

[19] A. N. Pfeiffer, C. Cirelli, M. Smolarski, D. Dimitrovski, M. Abu-Samha, L. B. Madsen, and U. Keller, Attoclock reveals natural coordinates of the laser-induced tunnelling current flow in atoms, Nature Phys. **8**, 76 (2012).

[20] N. Teeny, E. Yakaboylu, H. Bauke, and C. H. Keitel, Ionization time and exit momentum in strong-field tunnel ionization, Phys. Rev. Lett. **116**, 063003 (2016).

[21] H. Ni, U. Saalmann, and J. M. Rost, Tunneling exit characteristics from classical backpropagation of an ionized electron wave packet, Phys. Rev. A **97**, 013426 (2018).

[22] M. Han, P. Ge, J. Wang, Z. Guo, Y. Fang, X. Ma, X. Yu, Y. Deng, H. J. Wörner, Q. Gong, and Y. Liu, Complete characterization of sub-Coulomb-barrier tunnelling with phase-of-phase attoclock, Nature Photon. **15**, 765 (2021).

[23] M. Yu, K. Liu, M. Li, J. Yan, C. Cao, J. Tan, J. Liang, K. Guo, W. Cao, P. Lan, Q. Zhang, Y. Zhou, and P. Lu, Full experimental determination of tunneling time with attosecond-scale streaking method, Light Sci. Appl. **11**, 215 (2022).

[24] M. Yu, Y. Zhou, K. Liu, K. L. Liu, M. Li, and P. Lu, Radial-momentum-resolved measurement of the tunneling ionization time in attoclock experiments, Phys. Rev. A **106**, 053106 (2022).

[25] M. Yu, Y. Zhou, M. Li, and P. Lu, Probing the effect of orbital deformation on the atomic tunneling-ionization-time distribution by phase-of-the-phase spectroscopy, Phys. Rev. A **105**, 063103 (2022).

[26] S. Skruszewicz, J. Tiggesbäumker, K.-H. Meiwes-Broer, M. Arbeiter, T. Fennel, and D. Bauer, Two-color strong-field photoelectron spectroscopy and the phase of the phase, Phys. Rev. Lett. **115**, 043001 (2015).

[27] M. A. Almajid, M. Zabel, S. Skruszewicz, J. Tiggesbäumker, and D. Bauer, Two-color phase-of-the-phase spectroscopy in

the multiphoton regime, J. Phys. B: At. Mol. Opt. Phys. **50**, 194001 (2017).

[28] V. A. Tulsky, M. A. Almajid, and D. Bauer, Two-color phase-of-the-phase spectroscopy with circularly polarized laser pulses, Phys. Rev. A **98**, 053433 (2018).

[29] D. Würzler, S. Skruszewicz, A. M. Sayler, D. Zille, M. Möller, P. Wustelt, Y. Zhang, J. Tiggesbäumker, and G. G. Paulus, Accurate retrieval of ionization time by means of the phase-of-the-phase spectroscopy, and its limits, Phys. Rev. A **101**, 033416 (2020).

[30] V. A. Tulsky, B. Krebs, J. Tiggesbäumker, and D. Bauer, Revealing laser-coherent electron features using phase-of-the-phase spectroscopy, J. Phys. B: At. Mol. Opt. Phys. **53**, 074001 (2020).

[31] L. Guo, M. Zhao, W. Quan, X. J. Liu, and J. Chen, Breakdown of one-to-one correspondence between the photoelectron emission angle and the tunneling instant in the attoclock scheme, Optica **10**, 1316 (2023).

[32] I. Barth and O. Smirnova, Nonadiabatic tunneling in circularly polarized laser fields: Physical picture and calculations, Phys. Rev. A **84**, 063415 (2011).

[33] T. Herath, L. Yan, S. K. Lee, and W. Li, Strong-field ionization rate depends on the sign of the magnetic quantum number, Phys. Rev. Lett. **109**, 043004 (2012).

[34] I. Barth and O. Smirnova, Nonadiabatic tunneling in circularly polarized laser fields. II. Derivation of formulas, Phys. Rev. A **87**, 013433 (2013).

[35] I. Barth and M. Lein, Numerical verification of the theory of nonadiabatic tunnel ionization in strong circularly polarized laser fields, J. Phys. B: At. Mol. Opt. Phys. **47**, 204016 (2014).

[36] J. Kaushal, F. Morales, and O. Smirnova, Opportunities for detecting ring currents using an attoclock setup, Phys. Rev. A **92**, 063405 (2015).

[37] Q. Zhang, G. Basnayake, A. Winney, Y. F. Lin, D. Debrah, S. K. Lee, and W. Li, Orbital-resolved nonadiabatic tunneling ionization, Phys. Rev. A **96**, 023422 (2017).

[38] J. P. Wang and F. He, Tunneling ionization of neon atoms carrying different orbital angular momenta in strong laser fields, Phys. Rev. A **95**, 043420 (2017).

[39] K. Liu, H. Ni, K. Renziehausen, J.-M. Rost, and I. Barth, Deformation of atomic p± orbitals in strong elliptically polarized laser fields: Ionization time drifts and spatial photoelectron separation, Phys. Rev. Lett. **121**, 203201 (2018).

[40] S. Eckart, M. Kunitski, M. Richter, A. Hartung, J. Rist, F. Trinter, K. Fehre, N. Schlott, K. Henrichs, L. Schmidt, T. Jahnke, M. Schöfffer, K. Liu, I. Barth, J. Kaushal, F. Morales, M. Ivanov, O. Smirnova, and R. Dörner, Ultrafast preparation and detection of ring currents in single atoms, Nature Phys. **14**, 701 (2018).

[41] V. V. Serov, J. Cesca, and A. S. Kheifets, Numerical and laboratory attoclock simulations on noble-gas atoms, Phys. Rev. A **103**, 023110 (2021).

[42] G. F. Gribakin and M. Y. Kuchiev, Multiphoton detachment of electrons from negative ions, Phys. Rev. A **55**, 3760 (1997).

[43] S. F. C. Shearer and M. R. Monteith, Direct photodetachment of F^- by mid-infrared few-cycle femtosecond laser pulses, Phys. Rev. A **88**, 033415 (2013).

[44] G. F. Gribakin and S. M. K. Law, Comment on "Direct photodetachment of F^- by mid-infrared few-cycle femtosecond laser pulses", Phys. Rev. A **94**, 057401 (2016).

[45] J. H. Chen, X. R. Xiao, S. F. Zhao, and L. Y. Peng, Dependence of direct and rescattered photoelectron spectra of fluorine anions on orbital symmetry in a short laser pulse, Phys. Rev. A **101**, 033409 (2020).

[46] J. H. Chen, M. Han, X. R. Xiao, L. Y. Peng, and Y. Liu, Atomic-orbital-dependent photoelectron momentum distributions for F^- ions by orthogonal two-color laser fields, Phys. Rev. A **98**, 033403 (2018).

[47] J. H. Chen, L. C. Wen, and S. F. Zhao, Orbital-resolved photoelectron momentum distributions of F^- ions in a counter-rotating bicircular field, Opt. Express **31**, 5708 (2023).

[48] M. M. Liu, M. Li, Y. Shao, M. Han, Q. Gong, and Y. Liu, Effects of orbital and Coulomb potential in strong-field nonadiabatic tunneling ionization of atoms, Phys. Rev. A **96**, 043410 (2017).

[49] K. Liu, M. Li, W. Xie, K. Guo, S. Luo, J. Yan, Y. Zhou, and P. Lu, Revealing the effect of atomic orbitals on the phase distribution of an ionizing electron wave packet with circularly polarized two-color laser fields, Opt. Express **28**, 12439 (2020).

[50] G. S. J. Armstrong, D. D. A. Clarke, A. C. Brown, and H. W. van der Hart, Electron rotational asymmetry in strong-field photodetachment from F^- by circularly polarized laser pulses, Phys. Rev. A **99**, 023429 (2019).

[51] M. Y. Ivanov, M. Spanner, and O. Smirnova, Anatomy of strong field ionization, J. Mod. Opt. **52**, 165 (2005).